Light-Harvesting Nanoparticle Probes for FRET-Based Detection of Oligonucleotides with Single-Molecule Sensitivity

Nina Melnychuk, Sylvie Egloff, Anne Runser, Andreas Reisch, Andrey S Klymchenko

Light-harvesting nanoparticle probes for FRET-based detection of oligonucleotides with single-molecule sensitivity

Nina Melnychuk, Sylvie Egloff, Anne Runser, Andreas Reisch and Andrey S. Klymchenko*

Abstract: Controlling emission of bright luminescent nanoparticles by a single molecular recognition event remains an ultimate challenge in the design of ultrasensitive probes for biomolecules. It would require an efficient Förster resonance energy transfer (FRET) from the nanoparticle to a single acceptor at its surface, which is not realized to date. Here, we developed 20-nm light-harvesting nanoantenna particles, built of a tailor-made hydrophobic charged polymer poly(ethyl methacrylate-co-methacrylic acid), encapsulating ~1000 strongly coupled and highly emissive rhodamine dyes with their bulky counterion. Being 87-fold brighter than quantum dots QDots605 in single-particle microscopy (with 550-nm excitation), these DNA-functionalized nanoparticles exhibit >50% total FRET efficiency to a single hybridized FRET acceptor, a highly photostable carbopyronine dye (ATTO665). The obtained FRET nanoprobes enable single-molecule detection of short DNA and RNA, encoding a cancer marker, and imaging single hybridization events by an epi-fluorescence microscope with ultralow excitation irradiance close to ambient sunlight.

Introduction

Detection of biomolecular targets, such as nucleic acids, with single-molecule sensitivity is an ultimate goal in biosensing and biomedical diagnostics.[1] In optical detection of single molecules, the brightness of organic dyes is limited by molar absorption coefficients below 300,000 M^{-1} cm^{-1} and quantum yields below unity.[2] Therefore, the use of very high excitation powers (~1 kW cm^{-2}) and minimized detection volumes[1a, 3] is required in order to achieve good signal-to-background ratio. Plasmonic nanomaterials can address this problem by enhancing emission of single dyes in the hot spots,[1h, 4] in particular between two gold nanoparticles with strictly respected distances.[3b] This sophisticated system based on DNA origami enabled up to 100-300-fold signal amplification of single molecules.[3b, 5] However, so far, the reported biosensor for nucleic acids based on this concept can amplify the signal by 7-fold on the average.[6]

A promising amplification approach is to use bright luminescent nanoparticles (NPs)[7] as energy donors that pump excitation energy to a single dye molecule by Förster Resonance Energy Transfer (FRET).[8] However, nanoparticles are generally not efficient FRET donors, because their sizes are beyond the FRET operating range between 1 and 10 nm, defined by Förster radius (R_0).[9] Indeed, in case of quantum dots (QDots), 10-50 acceptor molecules are needed to ensure efficient FRET.[10] Similar large number of acceptors are also needed to ensure FRET from upconverting NPs (UCNPs)[11] and dye-doped silica NPs.[12] One way to go beyond the Förster radius is to use light-harvesting nanomaterials[13] where the strongly coupled energy donors communicate through excitation energy migration,[14] which allows transporting the energy through long distances up to the FRET acceptor. Previous works showed that energy migration can improve FRET efficiency in both dye-doped silica NPs[12b] and UCNPs.[15] Moreover, in conjugated polymers,[16] this approach enabled 25-100-fold signal amplification, although no single-molecule FRET-based detection was reported. New possibilities appeared with recently introduced giant light-harvesting nanoantenna,[8a] based on dye-loaded polymeric NPs.[17] In these NPs, dyes (R18, Scheme 1A) are loaded into polymer matrix at high concentration using bulky hydrophobic counterions (F5-TPB) that prevent dye self-quenching[18] and leaching (leakage) in biological media, including cells.[18c, 18d] Importantly, the high dye loading ensured short inter-fluorophore distance (~1 nm) controlled by the counterion, which enabled ultrafast dye-dye excitation energy migration on a time scale < 30 fs.[8a] In this system the excitation energy can freely migrate through the whole particle within the fluorescence lifetime until it reaches a donor close to the acceptor leading to FRET (Scheme 1A). Therefore, the energy can be transferred beyond R_0 from multiple donors to a single acceptor, providing a basis for signal amplification. Indeed, in our nanoantenna, ~10000 energy donors transferred energy to a single acceptor inside 60-nm particle (R_0 = 6.1 nm for R18 / cyanine 5 couple) leading to unprecedented signal amplification of >1000-fold.[8a] More recently, we functionalized 40 nm nanoantenna with nucleic acids and reported the first DNA-based biosensor featuring exceptional brightness of 3300 encapsulated R18 dyes and 75-fold signal amplification.[19] However, to achieve efficient FRET in these NPs, 23 acceptor dyes at the particle surface were needed, so that this system was still far from being able to detect single nucleic acid molecules. To the best of our knowledge, no luminescent NPs with a diameter above 10 nm are capable to undergo efficient FRET (i.e. >50%) to a single acceptor dye at the particle surface.

Herein, we overcame the problem of inefficient FRET in nanoparticle-based biosensors and developed a light-harvesting nanoantenna of 20 nm size, encapsulating ~1000 dyes with 52% fluorescence quantum yield (QY), which undergoes FRET with 51% efficiency to a single acceptor (ATTO665) at the DNA-functionalized surface. This new nanomaterial enabled preparation nanoprobes capable to switch their color in response to a single copy of RNA and DNA molecules and monitor in real time single hybridization events using a basic epi-fluorescence microscope with low excitation power density (irradiance) close to that of ambient sunlight.

Dr. Nina Melnychuk, Sylvie Egloff, Anne Runser, Dr. Andreas Reisch and Dr. Andrey S. Klymchenko*
Laboratoire de Bioimagerie et Pathologies, UMR 7021 CNRS, Faculté de Pharmacie, Université de Strasbourg
74, Route du Rhin, 67401 Illkirch, France
E-mail: andrey.klymchenko@unistra.fr

Supporting information for this article is given via a link at the end of the document.

Results and Discussion

Development of this single-molecule biosensor requires boosting FRET performance of our dye-loaded NPs. To this end, we need to design a polymer capable to assemble maximum number of dyes into a particle of optimal small size, while ensuring their efficient emission and excitation energy migration (Scheme 1A). Moreover, we need to find robust FRET acceptor able to collect energy from the whole particle without rapid photobleaching.

Then, based on a previously developed DNA-functionalization strategy,[19] the donor NPs should be modified with only a single FRET acceptor through a nucleic acid sensing unit. In our biosensor, azide-functionalized dye-loaded polymeric NPs are modified with two different oligonucleotide sequences (Scheme 1B): (i) excess of non-coding T20 to ensure NPs stability and (ii) a statistically one copy per particle of specific sequence (SurC), encoding a fragment of survivin, an important cancer marker.[20] The latter is hybridized with a shorter complementary DNA sequence (target competitive sequence, TCS) bearing the acceptor, which serves in the FRET displacement assay to detect the survivin DNA/RNA target (Scheme 1B).

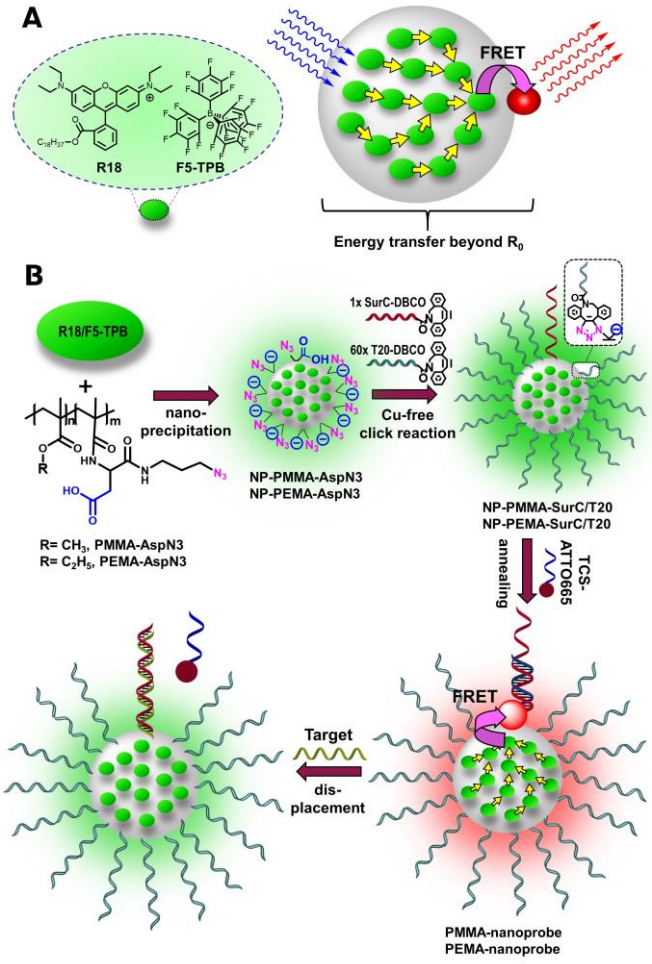

Scheme 1. Design of light-harvesting nanoprobe. (A) Principle of light-harvesting nanoantenna based on polymeric nanoparticle loaded with cationic dye (R18) and its bulky counterion (F5-TPB). FRET from donor dyes (green) to the acceptor (red) is shown by magenta arrow, whereas excitation energy migration within donor dyes is shown by yellow arrows. (B).Synthesis of the nanoprobes with a single TCS-Acceptor and their response to the target.

First, we searched for the best FRET acceptor, using previously developed dye-loaded donor NPs based on polymer PMMA-AspN3-1.6% (obtained from PMMA-MA with 1.6% of methacrylic acid).[19] Among ten tested acceptor dyes (Figure 1A) conjugated to DNA TCS, only positively charged and neutral (zwitterionic) cyanines (Cy5 and Cy5.5) and carbopyronines (ATTO647N and its close analogue ATTO665 with undisclosed structure), were found to provide a strong FRET signal after hybridization in the DNA nanoprobe. This signal was observed as an intense emission band around 650-750 nm compared to the FRET donor band of R18 dye around 590 nm (Figure 1B and S1). The number of hybridized acceptors per particle was also larger for these dyes (Table S1), probably because their duplexes were more stable than those bearing strongly anionic dyes.

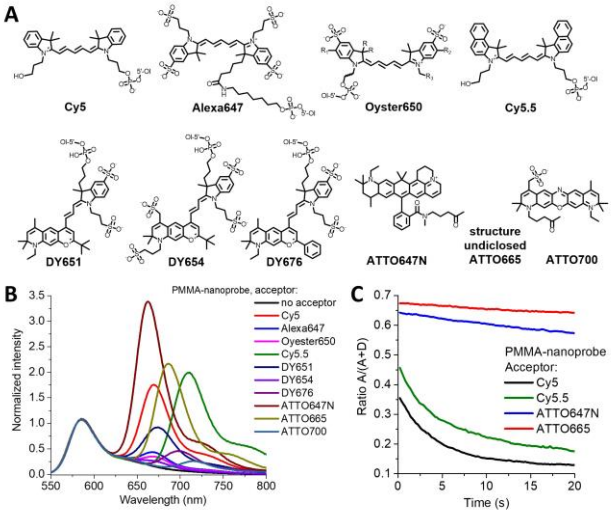

Figure 1. Search for the best FRET acceptor. A) Chemical structure of dyes conjugated with TCS and used as FRET-acceptors. B) Normalized fluorescence spectra of PMMA-nanoprobes (PMMA-AspN3-1.6% polymer) with different acceptors and 30 wt% R18/F5-TPB dye loading. 20 mM phosphate buffer containing 30 mM NaCl and 12 mM $MgCl_2$ was used. Excitation: 530 nm. C) Photobleaching kinetics of PMMA-nanoprobes formulated with different acceptors, immobilized on the glass surface and measured by microscopy. Excitation: 550 nm; power density: 0.41 W cm^{-2}.

Then, we tested the fluorescence response of the obtained four nanoprobes to the target DNA sequence encoding survivin fragment. The three nanoprobes based on Cy5, ATTO647N and ATTO665 showed complete replacement of the acceptor, resulting in loss of the acceptor emission (Figure S2). By contrast, Cy5.5-based acceptor showed residual FRET in the presence of the DNA target, showing that it remains non-specifically bound to the particle (Figure S3). We also compared photostability of the four nanoprobes in solution under laser irradiation (Figure S4). Remarkably, nanoprobes built of Cy5 or Cy5.5 dyes showed fast decay of the FRET acceptor signal, expressed as A/(A+D) ratio (Figure S4), whereas the signal from ATTO647N and ATTO665 was far more stable (half-life for ATTO665 and Cy5 was 3500 and 98 s, respectively). The significantly higher photostability of ATTO-based FRET acceptors was also confirmed at a single-particle level (half-life for ATTO665 and Cy5 was 128 and 3.7 s, respectively), using fluorescence microscopy of nanoprobes immobilized on the glass surface (Figure 1C, S5, S6). The observed much higher photostability for ATTO665 and

ATTO647N is probably due to their more rigid carbopyronine scaffold[21] compared to flexible Cy5 dyes prone to photoinduced reactions.[22] The obtained results suggest that, in comparison to Cy5, ATTO665 as FRET acceptor should provide ~35-fold more photons before photobleaching, which is important for construction of the single-molecule FRET nanoprobe.

After finding the best acceptor (ATTO665), we turned our attention to nanoantenna particle as the FRET donor. The primary approach to improve FRET donor efficiency of a particle together with its light-harvesting capacity is to minimize its size while keeping largest possible number of encapsulated donor dyes. Our earlier studies showed that smaller polymer NPs can be obtained by increasing the pH during nanoprecipitation[8a] or increasing the charge on the polymer.[23] In the first approach, we performed nanoprecipitation of PMMA-AspN3-1.6% at pH 9, which yielded NPs of 30 nm (Figure S7 A-B). However, the obtained DNA-functionalized nanoprobes required >8 acceptors per particle to achieve efficient FRET (Figure S7 C-D), so further decrease in the size was needed. Therefore, we increased the fraction of methacrylic acid units in PMMA-MA to 5 mol%, and further converted it into azide-carboxylate-bearing polymer PMMA-AspN3-5% (Scheme 1). Moreover, to compensate the increase in the fraction of polar carboxylates in the polymer, we replaced its methyl methacrylate unit with more hydrophobic ethyl methacrylate (PEMA-AspN3 polymer, Scheme 1, obtained from PEMA-MA with 1.6% of methacrylic acid). Nanoprecipitation of these polymers yielded dye-loaded NPs of 16 and 18 nm for PMMA-AspN3-5% and PEMA-AspN3, respectively (Figure 2 A-B).

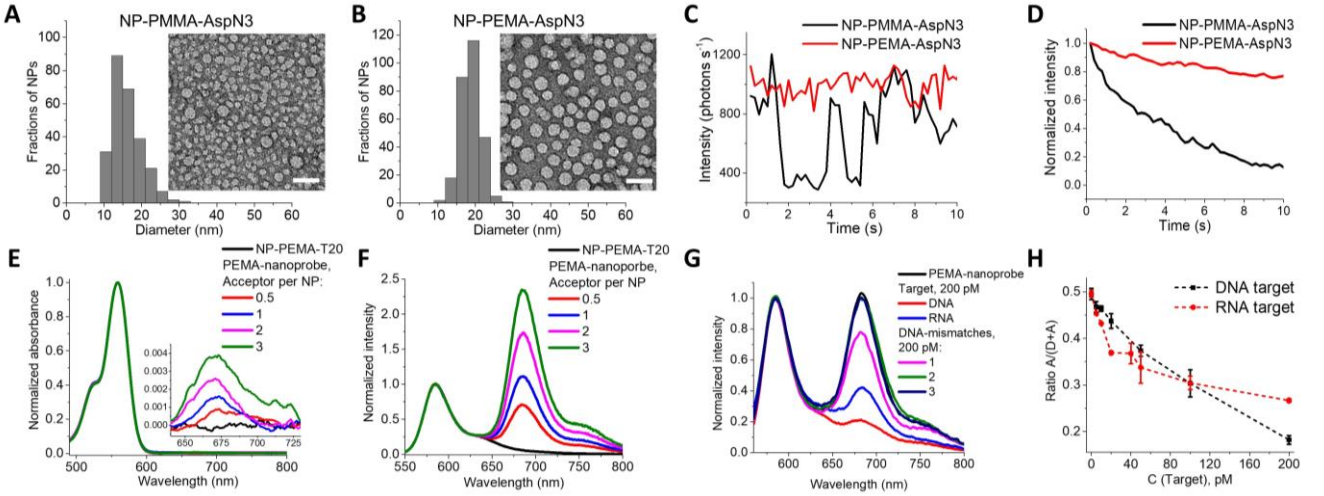

Figure 2. Development and evaluation of FRET nanoprobes. TEM images (scale bar 50 nm) and size distribution statistics for NPs of (A) PMMA-AspN3-5% and (B) PEMA-AspN3 polymers. C) Examples of single-particle intensity and (D) average intensity traces measured by microscopy for PMMA-AspN3-5% and PEMA-AspN3 NPs loaded with 50 wt% R18/F5-TPB. Excitation: 550 nm; power density: 0.41 W cm^{-2}. E) Absorbance and F) normalized fluorescence spectra of PEMA-nanoprobes (50 wt% R18/F5-TPB dye) hybridized with 0 (NP-PEMA-T20) and 0.3, 1 and 2 TCS-ATTO665 acceptor. G) Fluorescence response of PEMA-nanoprobe (20 pM of TCS-ATTO665) to survivin DNA and RNA targets (200 pM, 3 h incubation at 20 °C). DNA targets containing 1, 2, and 3 mismatches were tested at the same conditions. The spectra in (F) and (G) were normalized at the donor emission. H) FRET ratio, A/(A + D), of PEMA-nanoprobes (10 pM of TCS-ATTO665) vs target DNA and RNA concentration (3 h incubation at 20 °C). A and D are the pick intensities of the acceptor (at 665 nm) and the donor (at 580 nm), respectively. Error bars are standard deviation (n = 3). 20 mM phosphate buffer containing 30 mM NaCl and 12 mM $MgCl_2$ was systematically used.

Strikingly, PEMA-AspN3 NPs outdid PMMA-AspN3-5% NPs in all tested properties: (i) better size homogeneity according to TEM (Figure 1 A-B); (ii) higher fluorescence quantum yield (54 vs 31% at 30 wt% RhB/F5-TPB loading); (iii) 2.7-fold higher single particle brightness and (iv) much lower blinking and higher photostability (Figure 2 C-D, S8, Table S2). Thus, combining higher fraction of carboxylic groups with higher hydrophobicity of PEMA matrix enabled us to prepare very small dye-loaded NPs with drastically improved morphology and optical properties. As the particle brightness and the nanoantenna performance are directly linked to the dye loading, we varied it from 0 to 100 wt% with respect to the PEMA-AspN3 polymer. Even though QY values remained high (40-60%) for all loadings tested (Table S3), above 50 wt% the NPs showed lower single-particle photostability (Figure S9), probably linked to larger fraction of photo-induced dark states.[18b] Therefore, we selected 50 wt% as the optimal dye loading, exhibiting QY of 52%. In addition, increase in the dye loading till 50 wt% led to >100-fold drop in the fluorescence anisotropy (Figure S10), which suggested strong coupling of closely packed dyes inside NPs and efficient excitation energy migration within donor dyes independently from the acceptor.[14, 18a, 18b] This process should ensure long-distance excitation energy transport up to acceptor leading to an overall FRET beyond the Förster radius (Scheme 1A).[8a]

Next, in order to prepare the nanoprobes, we functionalized dye-loaded PEMA-AspN3 with oligonucleotides. It was important to increase the concentration of oligonucleotide-DBCO in order to ensure stability of these small DNA-NPs (Figure S11). In the obtained FRET nanoprobes we varied the number of hybridized TCS-ATTO665 acceptors from 0 to 3 (Figure S12) and found that FRET signal was sensitive to the addition of a single acceptor (Figure 2 E-F, S12). Indeed, the nanoprobe with a single acceptor exhibited remarkably high total FRET efficiency (51%), which implies efficient energy transfer from 980 donors inside the 20-nm particle to one acceptor at its surface, *i.e.* far beyond the Förster radius (R_0 = 6.7 nm, estimated for R18 and ATTO665 in our system, Table S3). The nanoprobe also showed high total fluorescence quantum yield (46%), while the amplification of acceptor emission (antenna effect) was 209 ± 16. This outstanding performance was highly reproducible in 5

independent preparations (Table S4). The obtained nanoprobes showed strong ratiometric response to the target survivin-encoding DNA and RNA sequences, where the target detection was associated with the loss of FRET signal (Figure 2G, S13). At 10-pM nanoprobe concentration, both DNA and RNA targets could be quantified at low pM concentrations (limit of detection was around 2 pM, estimated as three times of the standard deviations from the control, Figure 2H). In this case, the sensitivity is limited by slow oligonucleotide hybridization at these low concentrations. Incubation of the nanoprobe with the target DNA containing 1, 2 and 3 mismatches revealed high sequence specificity of the probe (Figure 2G). Moreover, the nanoprobe was found compatible with human serum. Indeed, the presence of 10% serum in phosphate buffer did not affect FRET signal of the nanoprobe and its response to the DNA target was only slightly decreased (Figure S14). These results, in line with the first generation DNA nanoprobe,[19] indicate that (i) both the donors and the acceptor remained within the nanoprobe without signs of leaching to serum and (ii) the strand displacement at the particle surface is weakly affected by the complex protein mixture.

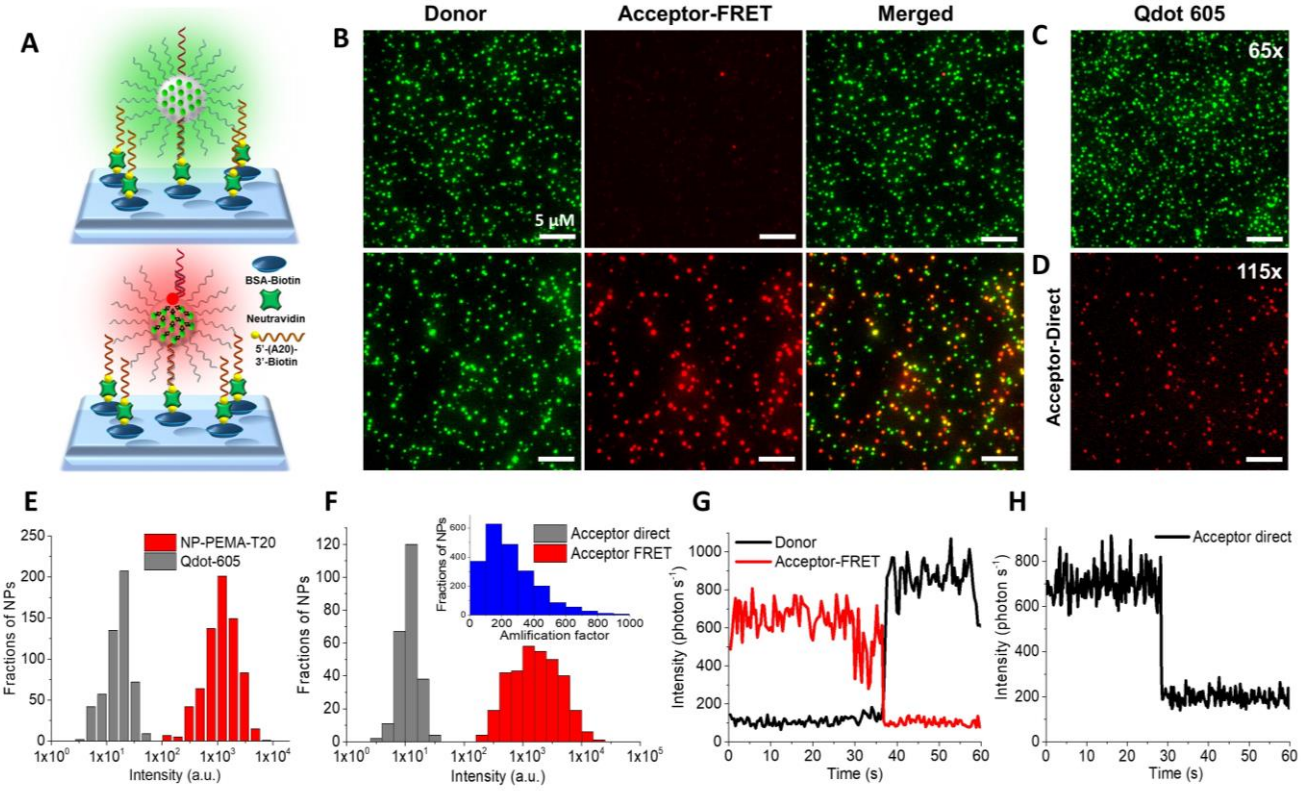

Figure 3. Characterization of nanoprobes at the single particle level. A) Scheme of PEMA-nanoprobe immobilization on a glass surface modified with BSA-biotin, neutravidin, and A20-biotin and B) Wide-field fluorescence microscopy of the immobilized NPs: donor, antenna-amplified acceptor and merged acceptor and donor Without (above) and with (under) TCS-ATTO665. Excitation wavelength was 550 nm with power density 0.24 W cm^{-2}. Signals from Donor and FRET-Acceptor were recorded at <640 and >640 nm, respectively. C) Wide-field fluorescence microscopy of the immobilized Qdot-605 excited at 550 nm with power density 15.4 W cm^{-2}. To obtain comparable signals excitation power density for QDot-605 was 65-fold higher than that for PEMA-T20. D) Wide-field fluorescence microscopy of PEMA nanoparticles at direct excitation of acceptor at 640 nm with power density 27.7 W cm^{-2}. Integration time was 400 ms. Histogram of single-particle intensity distribution for E) NP-PEMA-T20 and Qdot-605 and F) acceptor through direct excitation and nanoantenna energy transfer. Smaller graph represents a distribution histogram of amplification of FRET-Acceptor emission (antenna effect) by the nanoprobe at the single-particle level. At least 2000 NPs were analyzed in each case. Examples of single-particle intensity curves of FRET nanoprobe (G) excited at 550 nm with power density 0.24 W cm^{-2} and recorded at donor and acceptor channels and (H) direct excitation of acceptor at 640 nm on TIRF setup with power density 24.7 W cm^{-2}. 50 wt% R18/F5-TPB dye loading was systematically used.

Then, our DNA-functionalized NPs were studied at the single-particle level. PEMA-AspN3 NPs bearing only T20 were immobilized on A20-modified glass surface (Figure 3A) and compared with commercial Qdot-605 under the wide-field microscope at 550 nm excitation. We found that these 20-nm NPs were 87-fold brighter than Qdot-605 measured at the same conditions (Figure 3 A-C, E). This outstanding brightness for such a small particle size is explained by the high QY (52%) of 980 encapsulated rhodamine B derivatives, giving a theoretical brightness (number of dyes × extinction coefficient × QY) of 5.1 x 10^7 vs 5.8 x 10^5 M^{-1} cm^{-1} for Qdot-605.

FRET-based nanoprobes bearing a single acceptor showed emission in both donor (<640 nm) and acceptor (>640 nm) channels, whereas NPs without acceptor showed signal in the donor channel only (Figure 3B). Remarkably, the signal of acceptor excited through the nanoantenna (Acceptor-FRET) was 257 ± 30-fold stronger than that obtained by direct excitation (Acceptor-direct) (Figure 3D, F). This value matches well the antenna effect measured in solution, indicating that efficient energy transfer from a thousand of encapsulated dyes to a single acceptor at the NP surface results in the outstanding amplification. To the best of our knowledge, this is the largest antenna effect

ever reported for optical biosensors, including those based on plasmonics.

To verify the number of acceptors in our nanoprobe, we analyzed emission traces of the individual particles and quantified the number of single-molecule bleaching steps, which is a signature of the single acceptor per particle. When excited through nanoantenna (at 550 nm), we estimated that 61±4% of NPs contained acceptors, among which 48±5% demonstrated single bleaching step, corresponding to a single acceptor per nanoprobe. Moreover, 67±7% of single step acceptor photobleaching events were accompanied by recovery of the donor emission (Figure 3G, Table S5). This opposite switching behavior of donor and acceptor emission is typically observed in single-molecule FRET measurements.[24] However, in our nanoprobe a single acceptor switches on/off emission of the entire NP containing ~1000 of dyes. Direct excitation of the acceptor in a total internal reflection (TIRF) mode with 640 nm laser (Figure 3H) showed that 52 ± 4% of acceptors underwent the single bleaching step, confirming that a large fraction of nanoprobes bear a single acceptor.

The achieved >250-fold amplification of acceptor emission by the nanoantenna particles enabled single-molecule FRET detection (i.e. single-step bleaching of the acceptor and recovery of the donor) using simple epi-fluorescence microscope setup with a very low excitation irradiance comparable to ambient sunlight (36 mW cm^{-2}, Figure S15), which is >1000 times lower than that typically required for TIRF-based single-molecule detection. Then, we incubated the immobilized nanoprobes with increasing amounts of DNA target. Starting from 1 pM, individual particles switched their emission pseudo-color from red to green and the population of green species increased gradually (Figure S16). At the highest tested target concentration all nanoprobes switched their emission to green, showing the decrease in the FRET ratio parameter, A / (A + D) from 0.46 to 0.21 (Figure S17). The gradual switching indicates that the nanoprobe can be used for quantification of the nucleic acid targets. As our NPs bear only a single acceptor, the color switch of NPs corresponds to detection of the single nucleic acid molecule, so that we could practically calculate the number of target molecules hybridized with the nanoprobes. Therefore, we imaged a given area with immobilized nanoprobes and quantified the number of FRET-positive particles before and after incubation with DNA and RNA targets (Figure 4A). Without the target, no change in the number of FRET-positive nanoprobes was detected, whereas in case of DNA and RNA samples, 1433±87 and 768±24 particles, respectively, switched their color from red to green per 1600 μm^2 surface area (Figure 4 B-C). This “digital” detection of single-molecule targets correlated with corresponding drop in the average FRET ratio of NPs (Figure 4C, S18). Importantly, our nanoprobe enables detection of DNA/RNA targets with single-molecule sensitivity using basic epi-fluorescence microscope with excitation irradiance close to ambient sunlight (36 mW cm^{-2}), something that has not been achieved to date. Here, the minimal detectable concentration of oligonucleotides is not limited by nanoprobe sensitivity but by the hybridization kinetics.

Figure 4. Detection of oligonucleotides with single-molecule sensitivity using PEMA-nanoprobes immobilized on a glass surface. A) Schematic presentation of

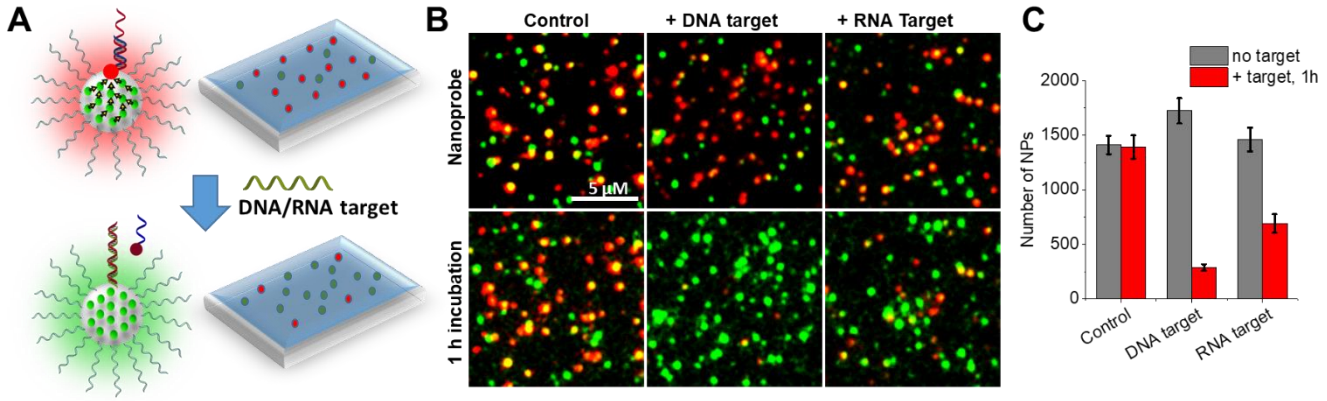

digital detection of single oligonucleotides. B) Wide-filed FRET images (two-color merged) and C) number of FRET-positive nanoprobes without and with 100 pM of DNA and RNA targets. The excitation wavelength was 550 nm with power density 0.036 W cm^{-2}, 60x oil objective. Integration time was 1 s. Error bars represent standard deviation of the mean from 3 images; ~2000 particles were analysed for each data point.

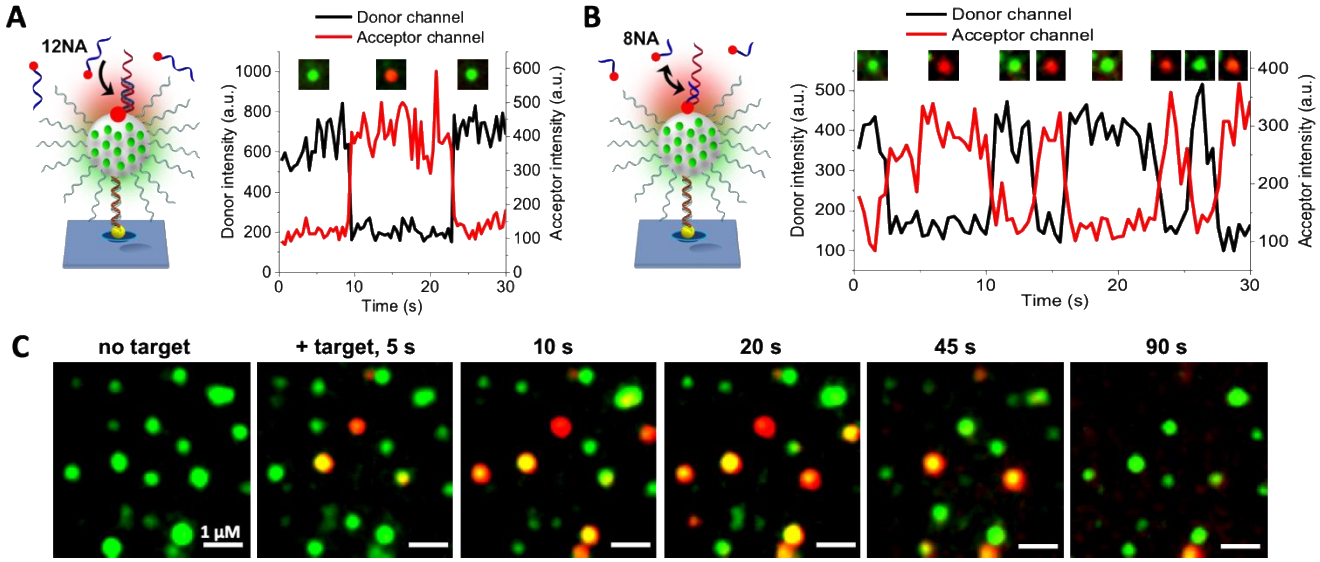

Figure 5. Imaging in real time single hybridization events using PEMA-SurC/T20 immobilized on a glass surface. Schemes of single-molecule irreversible (A) and reversible (B) hybridization of oligonucleotides TCS-ATTO665 of 12 nucleotides (12NA) and 8 nucleotides (8NA), respectively, with NP-PEMA-Surc/T20. Intensity traces of donor (black) and acceptor (red) of a single nanoprobe with addition of TCS-ATTO665 of 12NA (A) and 8NA (B) and corresponding two-color merged images of the same single particle. C) The same experiment as in (A): two-color merged images of a larger area at different times after addition of 50 nM of TCS-ATTO665. The excitation wavelength was 550 nm, 100x oil objective with power density 0.24 W cm^{-2}. Integration time was 400 ms. 50 wt% R18/F5-TPB dye loading was systematically used.

Finally, we challenged our nanoprobes in another key application: to image in real time the single hybridization events between two labelled oligonucleotides. In the first experiment, immobilized donor nanoparticles bearing a single capture sequence were treated with TCS-ATTO665 during the imaging (Figure 5A). After addition of TCS-ATTO665, initially green NPs turned into red and then returned back to green (Figure 5C, Video S1). In the intensity traces, the single step jump of the acceptor emission was accompanied by the drop of the donor one, which corresponded to the single hybridization event. Then, the acceptor dye got bleached which resulted in exactly opposite single step changes: drop of the acceptor and jump of the donor. In the second experiment, we added shorter (8mer) TCS-ATTO665 (Figure 5B), which was expected to bind reversibly to PEMA-NPs bearing complementary capture sequence, similar to what is done in DNA-PAINT imaging methods.[25] Remarkably, we were able to follow continuous process of binding-unbinding of the oligonucleotide-acceptor molecules to the donor NPs in our two-color images and the intensity traces, where donor and acceptor signals switched many times in the opposite way (Figure 5B, Video S2). The single-molecule nature of these switching evens was confirmed by observed single steps in the intensity traces of the acceptor directly excited (at 640 nm) in TIRF microscopy (Figure S19). Thus, these two experiments show that, owing to >250-amplification capability, our light-harvesting nanomaterial enables real-time detection of reversible and irreversible single oligonucleotide hybridization processes using a basic imaging setup with low excitation irradiance.

Conclusion

In conclusion, we developed an organic nanomaterial that breaks the FRET barrier in existing luminescent nanoparticle systems. It is based on a light-harvesting nanoantenna, where ~1000 of strongly coupled rhodamine dyes with 52% fluorescence quantum yield are confined within a 20-nm polymeric particle. The obtained nanoparticle, being as bright as 87 Qdots-605 in single-particle microscopy (excitation at 530 nm), shows unprecedented 51% total FRET efficiency to a single acceptor hybridized at the DNA-modified particle surface, generating antenna effect (amplification factor) of ~250. To the best of our knowledge, none of reported fluorescent nanoparticles can combine such high brightness and FRET efficiency to a single acceptor at the surface. High loading of bright rhodamine dyes with their bulky counterions (50 wt%) and a specially designed polymer in this nanoantenna ensure short interfluorophore distances with minimal self-quenching that lead to excitation energy migration within 1000 encapsulated dyes and further FRET to a single accepter. As a result, overall energy transfer takes place beyond the Förster radius with minimal energy losses. Thus, our 20-nm particle is an efficient FRET donor, like a small dye molecule, but it is ~1000-fold brighter. On the other hand, based on screening of 10 different FRET acceptors, we found that dyes of carbopyronine family (ATTO665 and ATTO647N) are up to 35-fold more photostable in our system than a Cy5 derivative. Based on these findings, we constructed FRET-based nanoprobe for nucleic acids operating by strand displacement mechanism, where we combined our DNA-functionalized nanoantenna particles (FRET donor) with a single hybridized ATTO665-based acceptor. Single-molecule microscopy of the nanoprobes confirmed efficient FRET to a single acceptor, where one photobleaching step of the acceptor

was accompanied by fluorescence intensity jump of entire particle containing ~1000 of dyes. The obtained nanoprobes enabled unprecedented FRET-based detection of single copies of short DNA and RNA as well as monitoring single oligonucleotide hybridization events by a simple epi-fluorescence microscope at low excitation irradiance (36 mW cm^{-2}), close to ambient sunlight. For comparison, conventional single-molecule detection techniques would require in this case >1000-fold higher excitation irradiance, TIRF microscopy and minimized detection volumes to achieve good signal-to-noise ratio.[1a, 3] The developed nanomaterials will drastically simplify single-molecule detection and open a route to FRET assays for ultrasensitive detection of biomolecular markers, especially microRNA, mRNA and DNA, which are present in biological samples at very low concentrations.[26] Finally, owing to their compatibility with complex biological media, such as serum, our nanoprobes will enable detection of nucleic acid targets directly in biological fluids and, ultimately, application to target detection and imaging in cells.[27]

Acknowledgements

This work was supported by the European Research Council ERC Consolidator grant BrightSens 648525. We thank Corinne Crucifix from the FRISBI platform for her help with the electron microscopy.

Keywords: light-harvesting nanoantenna • fluorescent nanoparticles • Förster resonance energy transfer • single-molecule detection • nucleic acids biosensor

[1] a) B. A. Flusberg, D. R. Webster, J. H. Lee, K. J. Travers, E. C. Olivares, T. A. Clark, J. Korlach, S. W. Turner, *Nat. Methods* **2010**, *7*, 461; b) J. Clarke, H. C. Wu, L. Jayasinghe, A. Patel, S. Reid, H. Bayley, *Nat. Nanotechnol.* **2009**, *4*, 265; c) R. K. Neely, P. Dedecker, J. I. Hotta, G. Urbanaviciute, S. Klimasauskas, J. Hofkens, *Chem. Sci.* **2010**, *1*, 453; d) K. Jo, D. M. Dhingra, T. Odijk, J. J. de Pablo, M. D. Graham, R. Runnheim, D. Forrest, D. C. Schwartz, *Proc. Natl. Acad. Sci. U. S. A.* **2007**, *104*, 2673; e) L. A. Neely, S. Patel, J. Garver, M. Gallo, M. Hackett, S. McLaughlin, M. Nadel, J. Harris, S. Gullans, J. Rooke, *Nat. Methods* **2006**, *3*, 41; f) M. D. Baaske, M. R. Foreman, F. Vollmer, *Nat. Nanotechnol.* **2014**, *9*, 933; g) B. Hornblower, A. Coombs, R. D. Whitaker, A. Kolomeisky, S. J. Picone, A. Meller, M. Akeson, *Nat. Methods* **2007**, *4*, 315; h) J. D. Spitzberg, A. Zrehen, X. F. van Kooten, A. Meller, *Adv. Mater.* **2019**, *31*, 1900422.

[2] a) L. D. Lavis, R. T. Raines, *ACS Chem. Biol.* **2014**, *9*, 855; b) G. T. Dempsey, J. C. Vaughan, K. H. Chen, M. Bates, X. W. Zhuang, *Nat. Methods* **2011**, *8*, 1027.

[3] a) M. J. Levene, J. Korlach, S. W. Turner, M. Foquet, H. G. Craighead, W. W. Webb, *Science* **2003**, *299*, 682; b) G. P. Acuna, F. M. Möller, P. Holzmeister, S. Beater, B. Lalkens, P. Tinnefeld, *Science* **2012**, *338*, 506; c) M. Sauer, J. Hofkens, J. Enderlein, *Handbook of Fluorescence Spectroscopy and Imaging: From Ensemble to Single Molecules*, Wiley-VCH, **2011**.

[4] a) K. Aslan, I. Gryczynski, J. Malicka, E. Matveeva, J. R. Lakowicz, C. D. Geddes, *Curr. Opin. Biotechnol.* **2005**, *16*, 55; b) Y. Wang, B. Liu, A. Mikhailovsky, G. C. Bazan, *Adv. Mater.* **2010**, *22*, 656; c) A. G. Brolo, *Nat. Photonics* **2012**, *6*, 709; d) F. Zang, Z. Su, L. Zhou, K. Konduru, G. Kaplan, S. Y. Chou, *Adv. Mater.* **2019**, *31*, 1902331.

[5] A. Puchkova, C. Vietz, E. Pibiri, B. Wunsch, M. S. Paz, G. P. Acuna, P. Tinnefeld, *Nano Lett.* **2015**, *15*, 8354.

[6] S. E. Ochmann, C. Vietz, K. Trofymchuk, G. P. Acuna, B. Lalkens, P. Tinnefeld, *Anal. Chem.* **2017**, *89*, 13000.

[7] a) P. D. Howes, R. Chandrawati, M. M. Stevens, *Science* **2014**, *346*, 1247390; b) O. S. Wolfbeis, *Chem. Soc. Rev.* **2015**, *44*, 4743.

[8] a) K. Trofymchuk, A. Reisch, P. Didier, F. Fras, P. Gilliot, Y. Mely, A. S. Klymchenko, *Nat. Photonics* **2017**, *11*, 657; b) F. J. Hofmann, M. I. Bodnarchuk, L. Protesescu, M. V. Koyalenko, J. M. Lupton, J. Vogelsang, *J. Phys. Chem. Lett.* **2019**, *10*, 1055; c) C. Q. Li, J. Zhang, S. Y. Zhang, Y. Zhao, *Angew. Chem.-Int. Edit.* **2019**, *58*, 1643; d) J. Su, et al., *Angew. Chem. Int. Ed.* **2016**, *55*, 3662.

[9] K. E. Sapsford, L. Berti, I. L. Medintz, *Angew. Chem. Int. Ed.* **2006**, *45*, 4562.

[10] a) N. Hildebrandt, C. M. Spillmann, W. R. Algar, T. Pons, M. H. Stewart, E. Oh, K. Susumu, S. A. Diaz, J. B. Delehanty, I. L. Medintz, *Chem. Rev.* **2017**, *117*, 536; b) I. L. Medintz, A. R. Clapp, H. Mattoussi, E. R. Goldman, B. Fisher, J. M. Mauro, *Nat. Mater.* **2003**, *2*, 630; c) C. Y. Zhang, H. C. Yeh, M. T. Kuroki, T. H. Wang, *Nat. Mater.* **2005**, *4*, 826.

[11] a) O. Dukhno, F. Przybilla, M. Collot, A. Klymchenko, V. Pivovarenko, M. Buchner, V. Muhr, T. Hirsch, Y. Mely, *Nanoscale* **2017**, *9*, 11994; b) M. D. Wisser, S. Fischer, C. Siefe, A. P. Alivisatos, A. Salleo, J. A. Dionne, *Nano Lett.* **2018**, *18*, 2689.

[12] a) S. Bonacchi, D. Genovese, R. Juris, M. Montalti, L. Prodi, E. Rampazzo, N. Zaccheroni, *Angew. Chem. Int. Ed.* **2011**, *50*, 4056; b) D. Genovese, E. Rampazzo, S. Bonacchi, M. Montalti, N. Zaccheroni, L. Prodi, *Nanoscale* **2014**, *6*, 3022.

[13] a) S. Kundu, A. Patra, *Chem. Rev.* **2017**, *117*, 712; b) J. J. Li, Y. Chen, J. Yu, N. Cheng, Y. Liu, *Adv. Mater.* **2017**, *29*, 1701905; c) S. Guo, Y. Song, Y. He, X.-Y. Hu, L. Wang, *Angew. Chem. Int. Ed.* **2018**, *57*, 3163; d) L. Xu, Z. Wang, R. Wang, L. Wang, X. He, H. Jiang, H. Tang, D. Cao, B. Z. Tang, *Angew. Chem. Int. Ed.* **2019**, *0*.

[14] R. Camacho, D. Tauber, I. C. Scheblykin, *Adv. Mater.* **2019**, *31*, 30.

[15] R. Deng, J. Wang, R. Chen, W. Huang, X. Liu, *J. Am. Chem. Soc.* **2016**, *138*, 15972.

[16] a) W. B. Wu, G. C. Bazan, B. Liu, *Chem* **2017**, *2*, 760; b) Y. S. Wang, B. Liu, *Chem. Commun.* **2007**, 3553; c) B. S. Gaylord, A. J. Heeger, G. C. Bazan, *Proc. Natl. Acad. Sci. U. S. A.* **2002**, *99*, 10954; d) S. W. Thomas, G. D. Joly, T. M. Swager, *Chem. Rev.* **2007**, *107*, 1339; e) S. Rochat, T. M. Swager, *ACS Appl. Mater. Interfaces* **2013**, *5*, 4488; f) Y. Jiang, J. McNeill, *Chem. Rev.* **2017**, *117*, 838; g) S. Wang, G. C. Bazan, *Adv. Mater.* **2003**, *15*, 1425.

[17] A. Reisch, A. S. Klymchenko, *Small* **2016**, *12*, 1968.

[18] a) A. Reisch, P. Didier, L. Richert, S. Oncul, Y. Arntz, Y. Mely, A. S. Klymchenko, *Nat. Commun.* **2014**, *5*, 4089; b) A. Reisch, K. Trofymchuk, A. Runser, G. Fleith, M. Rawiso, A. S. Klymchenko, *ACS Appl. Mater. Interfaces* **2017**, *9*, 43030; c) B. Andreiuk, A. Reisch, E. Bernhardt, A. S. Klymchenko, *Chem. Asian. J.* **2019**, *14*, 836; d) B. Andreiuk, A. Reisch, M. Lindecker, G. Follain, N. Peyrieras, J. G. Goetz, A. S. Klymchenko, *Small* **2017**, *13*, 1701582.

[19] N. Melnychuk, A. S. Klymchenko, *J. Am. Chem. Soc.* **2018**, *140*, 10856.

[20] A. E. Prigodich, D. S. Seferos, M. D. Massich, D. A. Giljohann, B. C. Lane, C. A. Mirkin, *Acs Nano* **2009**, *3*, 2147.

[21] K. Kolmakov, V. N. Belov, C. A. Wurm, B. Harke, M. Leutenegger, C. Eggeling, S. W. Hell, *European J. Org. Chem.* **2010**, 3593.

[22] a) T. Ha, P. Tinnefeld, in *Annu. Rev. Phys. Chem., Vol. 63* (Eds.: M. A. Johnson, T. J. Martinez), Annual Reviews, Palo Alto, **2012**, pp. 595; b) J. Widengren, P. Schwille, *J. Phys. Chem. A* **2000**, *104*, 6416.

[23] A. Reisch, D. Heimburger, P. Ernst, A. Runser, P. Didier, D. Dujardin, A. S. Klymchenko, *Adv. Funct. Mater.* **2018**, *28*.

[24] a) B. Hellenkamp, et al., *Nat. Methods* **2018**, *15*, 669; b) R. Roy, S. Hohng, T. Ha, *Nat. Methods* **2008**, *5*, 507.

[25] R. Jungmann, M. S. Avendano, J. B. Woehrstein, M. J. Dai, W. M. Shih, P. Yin, *Nat. Methods* **2014**, *11*, 313.

[26] A. B. Chinen, C. M. Guan, J. R. Ferrer, S. N. Barnaby, T. J. Merkel, C. A. Mirkin, *Chem. Rev.* **2015**, *115*, 10530.

[27] a) D. Samanta, S. B. Ebrahimi, C. A. Mirkin, *Adv. Mater.* **2019**, https://doi.org/10.1002/adma.201901743, 1901743; b) K. Chakraborty, A. T. Veetil, S. R. Jaffrey, Y. Krishnan, in *Annu. Rev. Biochem., Vol. 85* (Ed.: R. D. Kornberg), Annual Reviews, Palo Alto, **2016**, pp. 349; c) D. S. Seferos, D. A. Giljohann, H. D. Hill, A. E. Prigodich, C. A. Mirkin, *J. Am. Chem. Soc.* **2007**, *129*, 15477.

RESEARCH ARTICLE

Light-harvesting nanoprobes are developed based on polymeric nanoparticles encapsulating ~1000 strongly coupled and highly emissive dyes capable to undergo >50% FRET to a single acceptor at the DNA-functionalized particle surface. This nanomaterial enables unprecedented detection of single copies of DNA/RNA by a simple epi-fluorescence microscope with ultralow excitation power close to ambient sunlight.

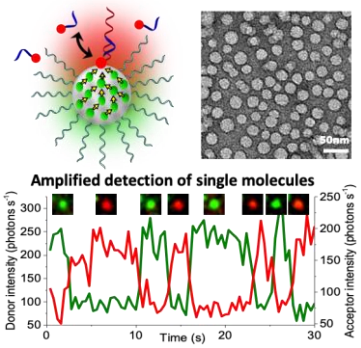

*Nina Melnychuk, Sylvie Egloff, Anne Runser, Andreas Reisch and Andrey S. Klymchenko**

Page No. – Page No.

Light-harvesting nanoprobes